Block Copolymer-Assisted Synthesis of Mesoporous, Multicomponent Oxides by Nonhydrolytic, Thermolytic Decomposition of Molecular Precursors in Nonpolar Media

Joshua W. Kriesel, Melissa S. Sander, and T. Don Tilley*

Department of Chemistry, University of California, Berkeley, Berkeley, California 94720-1460, and Chemical Sciences Division, Lawrence Berkeley Laboratory, 1 Cyclotron Road, Berkeley, California 94720

Received January 25, 2001. Revised Manuscript Received April 17, 2001

A general route for the synthesis of homogeneous mixed-element oxides, based on the use of block polyalkylene oxide copolymers and single-source molecular precursors, is described. Thermolytic decomposition of the molecular precursors in the presence of an anhydrous solution of the block copolymer (in toluene) led to monolithic gels. The polymeric structure-directing agent was then removed by calcination at 500 °C for 3 h under O_2. The generality of this synthetic approach is demonstrated with the molecular precursors $Zr[OSi(O^tBu)_3]_4$, $(EtO)_2Ta[OSi(O^tBu)_3]_3$, $Fe[OSi(O^tBu)_3]_3 \cdot THF$ and $[Al(O^iPr)_2O_2P(O^tBu)_2]_4$, which have been converted to the corresponding mesostructured materials $ZrO_2 \cdot 4SiO_2$, $Ta_2O_5 \cdot 6SiO_2$, $Fe_2O_3 \cdot 6SiO_2$, and $AlPO_4$ (denoted **UCB1-ZrSi**, **UCB1-TaSi**, **UCB1-FeSi**, and **UCB1-AlP**, respectively). These mesostructured materials, characterized by TEM, XRD, N_2 porosimetry, EDX, and NMR spectroscopy, exhibit wormholelike pore structures, high surface areas, and narrow pore size distributions.

Introduction

There is currently strong interest in the use of supramolecular species to control the nanoarchitecture of materials.[1] In this regard, a primary focus is on development of efficient general methods for organizing building blocks with interesting elemental compositions into predetermined shapes and length scales. One method for the controlled generation of materials with well-defined nanoarchitectures involves use of polymer and/or surfactant templates as structure-directing agents.[2−4] Mesoporous oxides prepared this way exhibit narrow pore size distributions with pore sizes ranging from 20 to 300 Å and often highly ordered pore structures. In these materials, the polymers or surfactant templates guide formation of the mesoporous oxides via electrostatic and hydrogen-bonding interactions. While many mesoporous silicas have been described, relatively few reports on the use of structure-directing agents to synthesize transition metal-containing mesoporous materials have appeared.[5,6] Furthermore, accounts of related structures with more complicated stoichiometries (e.g., bicomponent oxides) are even more rare.[6] Clearly, synthetic methods that allow variations in the composition of nanostructured solids, and access to complex stoichiometries for such materials, would greatly increase the potential for technological applications.

Intense research efforts in the template-directed synthesis of mesoporous materials were sparked by a report from scientists at Mobil Corp.,[2a] which described the preparation of MCM-41, a class of silicate materials with a hexagonal pore structure (pore radii = 10−50 Å) prepared using long chain quaternary ammonium cation surfactants as the structure-directing agents. Additionally, analogous anionic[7] and neutral[3b] amine-based surfactants have been used as effective templates

(1) Stupp, S. I.; LeBonheur, V.; Walker, K.; Li, L. S.; Huggins, K. E.; Keser, M.; Amstutz, A. *Science* **1997**, *276*, 384.

(2) (a) Kresge, C. T.; Leonowicz, M. E.; Roth, W. J.; Vartuli, J. C.; Beck, J. S. *Nature* **1992**, *359*, 710. (b) Beck, J. S.; Vartuli, J. C.; Roth, W. J.; Leonowicz, M. E.; Kresge, C. T.; Schmitt, K. T.; Chu, C. T. W.; Olson, D. H.; Sheppard, E. W.; McCullen, S. B.; Higgins, J. B.; Schlenker, J. L. *J. Am. Chem. Soc.* **1992**, *114*, 10834.

(3) (a) Zhao, D.; Feng, J.; Huo, Q.; Melosh, N.; Fredrickson, G. H.; Chmelka, B. F.; Stucky, G. D. *Science* **1998**, *279*, 548. (b) Tanev, P. T.; Pinnavaia, T. J. *Science* **1995**, *267*, 865.

(4) (a) Attard, G. S.; Glyde, J. C.; Göltner, C. G. *Nature* **1995**, *378*, 366. (b) Templin, M.; Franck, A.; Chesne, A. D.; Leist, H.; Zgang, Y.; Ulrich, R.; Schädler, U.; Wiesner, U. *Science* **1997**, *278*, 1795.

(5) (a) Tian, Z.; Tong, W.; Wang, J.; Duan, N.; Krishnan, V. V.; Suib, S. L. *Science* **1997**, *276*, 926. (b) Bagshaw, S. A.; Pinnavaia, T. J. *Angew. Chem., Int. Ed. Engl.* **1996**, *35*, 1102. (c) Vaudry F.; Khodabandeh S.; Davis M. E. *Chem. Mater.* **1996**, *8*, 1451. (d) Antonelli, D. M.; Ying, J. Y. *Angew. Chem., Int. Ed. Engl.* **1995**, *34*, 2014. (e) Putnam, R. L.; Nakagawa, N.; McGrath, K. M.; Yao, N.; Aksay, I. A.; Gruner, S. M.; Navrotsky, A. *Chem. Mater.* **1997**, *9*, 2690. (f) Ciesla, U.; Schacht, S.; Stucky, G. D.; Unger, K. K.; Schüth, F. *Angew. Chem., Int. Ed. Engl.* **1996**, *35*, 541. (g) Knowles, J. A.; Hudson, M. J. *Chem. Commun.* **1995**, 2083. (h) Kim, A.; Bruinsma, P.; Chen, Y.; Wang, L.; Liu, J. *Chem. Commun.* **1997**, 161. (i) Pacheco, G.; Zhao, E.; Garcia, A.; Sklyarov, A.; Fripiat, J. J. *Chem. Commun.* **1997**, 491. (j) Wong, M. S.; Ying, J. Y. *Chem. Mater.* **1998**, *10*, 2067. (k) Liu, P.; Liu, J.; Sayari, A. *Chem. Commun.* **1997**, 557. (l) Severin, K. G.; Abdel-Fattah, T. M.; Pinnavaia, T. J. *Chem. Commun.* **1998**, 1471. (m) Attard, G. S.; Barlett, P. N.; Coleman, N. R. B.; Elliott, J. M.; Owen, J. R.; Wang, J. H. *Science* **1997**, *278*, 838. (n) Ulagappan, N.; Rao, C. N. R. *Chem. Commun.* **1996**, 1685. (o) Braun, P. V.; Osenar, P.; Stupp, S. I. *Nature* **1996**, *380*, 325. (p) Antonelli, D. M.; Ying, J. Y. *Chem. Mater.* **1996**, *8*, 874. (q) Khushalani, D.; Dag, O.; Ozin, G. A.; Kuperman, A. *J. Mater. Chem.* **1999**, *9*, 1491.

(6) (a) Yang, P.; Zhao, D.; Margolese, D. I.; Chmelka, B. F.; Stucky, G. D. *Nature* **1998**, *396*, 512. (b) Yang, P.; Zhao, D.; Margolese, D. I.; Chmelka, B. F.; Stucky, G. D. *Chem. Mater.* **1999**, *11*, 2813.

10.1021/cm010068t CCC: $20.00 © 2001 American Chemical Society
Published on Web 06/14/2001

to make silicas with hexagonal pore structures. Neutral templating routes appear to generally have the advantage of yielding materials with thicker framework walls and, hence, more stable oxide structures.[8] Nonetheless, neutral alkylamines are not well suited for large scale synthesis of mesostructured materials since they are both costly and toxic.

A recently developed method for the preparation of mesoporous oxides employs nonionic block copolymers in conjunction with the sol−gel hydrolysis of metal alkoxides.[4,8−10] This protocol is attractive due to the ready availability of various metal alkoxides and block copolymers. Further, many block copolymers, particularly those containing poly(alkene oxide) (PEO) blocks, are inexpensive and biodegradable. The large number of reports on the use of such polymeric templates reflect their synthetic utility and the fact that mesoporous oxides prepared from them possess thick (and therefore more stable) framework walls. Pinnavaia and co-workers hydrolyzed metal alkoxide precursors in the presence of PEO block copolymers under neutral solvent conditions to obtain silica and alumina with disordered hexagonal and "wormhole" type pore structures.[8] Stucky and co-workers have isolated well-ordered hexagonal and cubic mesoporous silicas by hydrolyzing TEOS (tetraethyl orthosilicate) under highly acidic conditions (pH < 1) in the presence of PEO surfactants.[3a]

The mesoporous silicas described above are typically isolated as powders composed of micrometer-sized particles. Obviously, to realize applications for mesoporous materials in such areas as filtration or electronics, more elaborate processing techniques are required that allow, for example, monolith formation.[11] Toward that end, several recent publications have reported the isolation of monolithic mesoporous silicas using block copolymer liquid crystal phases.[9c,12,13]

Although a wide variety of template-directed mesoporous silicas have been isolated, relatively few nonsilica oxides have been reported.[6] Additionally, almost no reports describe the synthesis of mixed-element oxides that incorporate metals into the framework walls. However, Stucky et al. have used the hydrolyses of metal chlorides in ethanolic solvents in the presence of diblock and triblock poly(ethylene oxide) copolymers to produce a variety of large-pore metal oxides with semicrystalline frameworks.[6] Additionally, they have used this method to synthesize a few mixed-metal oxides by combining two metal chlorides (e.g. $SiCl_4$ and $TiCl_4$) with an ethanol solution of the block copolymer. Such materials appear to be somewhat homogeneous, but this issue is difficult to address given the lack of general methods for quantitatively observing the M−O−M′ heterolinkages. The issue of homogeneity (i.e., the concentration of heterolinkages) in such materials is quite relevant, since new properties are expected to result from interactions of the different elements in a mixed oxide. Unfortunately, the cohydrolysis approach to mixed-element oxides is plagued with the inherently different hydrolysis rates exhibited by any two precursor compounds. Thus, use of independent precursors in a cohydrolysis will invariably lead to the formation of at least some M−O−M homolinkages.[14,15]

For several years we have been exploring a new route to mixed-element oxide materials based on the use of oxygen-rich "single-source molecular precursors".[16] These molecular building blocks enforce a well-defined stoichiometry for the targeted mixed-element oxides materials. This synthetic strategy is based on our findings that the thermolysis, at relatively mild temperatures (100−180 °C), of metal derivatives of $-OSi(O^tBu)_3$ and $-O(O)P(O^tBu)_2$ involves clean elimination of isobutylene and water to yield $M_xSi_yO_z$ and $M_xP_yO_z$ materials, respectively. This synthetic method allows for formation of oxide materials with a high degree of homogeneity, because the elements to be incorporated into the material are initially part of the same molecule and bonded only to oxygen. The thermolytic conversion to materials is nonhydrolytic, in that it does not require added water for network formation. This feature has allowed us to carry out thermolytic transformations of molecular precursors in nonpolar organic solvents (e.g. toluene, octane, and mesitylene), which minimize the collapse of the network pore structure upon desiccation of the wet gel and allow for the isolation of high surface area materials.[14,17] Using the *thermolytic molecular precursor route* described above, we have previously reported the synthesis of a wide variety of homogeneous mixed-element oxide materials [e.g., $MO_2{\cdot}4SiO_2$ (M = Ti, Zr, Hf), $CuO{\cdot}nSiO_2$, $3Al_2O_3{\cdot}2SiO_2$, $Fe_2O_3{\cdot}6SiO_2$, $M_2O_5{\cdot}6SiO_2$ (M = Ta, Nb), $AlPO_4$, $ZrO_2{\cdot}P_2O_5$, $Zn(PO_3)_2$].[16,18] Typically these materials have broad pore size distributions which arise from a high degree of textural mesoporosity. Thus, to use these materials as, for example, catalyst supports or sensors, it is highly desirable to tailor their nanoscopic architecture (i.e. pore structure) for specific applications.

Herein we report the use of nonionic amphiphilic poly(alkylene oxide) block copolymers (e.g., $HO(CH_2$-

(7) Huo, Q.; Margolese, D. I.; Ciesia, F. P.; Gier, T. E.; Sieger, P.; Leon, R.; Petroff, P. M.; Schüth, F.; Stucky, G. D. *Nature* **1994**, *368*, 317.

(8) Bagshaw, S. A.; Prouzet, E.; Pinnavaia, T. J. *Science* **1995**, *269*, 1242.

(9) (a) Göltner, C. G.; Antonietti, M. *Adv. Mater.* **1997**, *9*, 431. (b) Antonietti, M.; Göltner, C. *Angew. Chem., Int. Ed. Engl.* **1997**, *36*, 910. (c) Göltner, C. G.; Henke, S.; Weissenberger, M. C.; Antonietti, M. *Angew. Chem., Int. Ed. Engl.* **1997**, *37*, 6613.

(10) (a) Bagshaw, S. A. *Chem. Commun.* **1999**, 271. (b) Yu, C.; Yu, Y.; Zhao, D. *Chem. Commun.* **2000**, 575.

(11) McGrath, K. M.; Dabbs, D. M.; Yao, N.; Aksay, A.; Gruner, S. M. *Science* **1997**, *277*, 552.

(12) (a) Feng, P.; Bu, X.; Stucky, G. D.; Pine, D. J. *J. Am. Chem. Soc.* **2000**, *122*, 994. (b) Melosh, N. A.; Lipic, P.; Bates, F. S.; Wudl, F.; Stucky, G. D.; Fredrickson, G. H.; Chmelka, B. F. *Macromolecules* **1999**, *32*, 4332.

(13) Melosh, N. A.; Davidson, P.; Chmelka, B. F. *J. Am. Chem. Soc.* **2000**, 122, 823.

(14) Brinker, C. J.; Scherer, G. W. *Sol−Gel Science: The Physics and Chemistry of Sol−Gel Processing*; Academic Press, Inc.: San Diego, CA, 1990.

(15) (a) Schubert, U. *J. Chem. Soc., Dalton Trans.* **1996**, 3343. (b) Schubert, U.; Hüsing, N.; Lorenz, A. *Chem. Mater.* **1995**, *7*, 2010. (c) Schmidt, H.; Scholze, H.; Kaiser, A. *J. Non-Cryst. Solids* **1982**, *48*, 65.

(16) (a) Terry, K. W.; Tilley, T. D. *Chem. Mater.* **1991**, *3*, 1001. (b) Terry, K. W.; Gantzel, P. K.; Tilley, T. D. *Chem. Mater.* **1992**, *4*, 1290. (c) Terry, K. W.; Gantzel, P. K.; Tilley, T. D. *Inorg. Chem.* **1993**, *32*, 5402. (d) Terry, K. W.; Lugmair, C. G.; Gantzel, P. K.; Tilley, T. D. *Chem. Mater.* **1996**, *8*, 274. (e) Lugmair, C. G.; Tilley, T. D.; Rheingold, A. L. *Chem. Mater.* **1997**, *9*, 339. (f) Su, K.; Tilley, T. D. *Chem. Mater.* **1997**, *9*, 588. (g) Su, K.; Tilley, T. D.; Sailor, M. J. *J. Am. Chem. Soc.* **1996**, *118*, 3459. (h) Terry, K. W.; Lugmair, C. G.; Tilley, T. D. *J. Am. Chem. Soc.* **1997**, *119*, 9745. (i) Lugmair, C. G; Tilley, T. D.; Rheingold, A. L. *Chem. Mater.* **1999**, *11*, 1615. (j) Kriesel, J. W.; Sander, M. S.; Tilley, T. D. *Adv. Mater.* **2001**, *13*, 331.

(17) Kriesel, J. W.; Tilley, T. D. *Chem. Mater.* **2000**, *12*, 1171.

(18) Lugmair, C. G.; Ph.D. Thesis, U.C. Berkeley, Berkeley, CA, 1997.

$CH_2O)_{106}(CH_2CH(CH_3)O)_{70}(CH_2CH_2O)_{106}H$, abbreviated as $EO_{106}PO_{70}EO_{106}$) as structure-directing agents for the synthesis of homogeneous mixed-element oxides from multicomponent molecular precursors. These materials are synthesized in nonpolar organic media and are isolated as monolithic gels. Following calcination (500 °C, O_2, 3 h), mixed-element oxide materials are obtained with narrow pore size distributions, high surface areas and thick framework walls. The template-directed synthesis of mixed-element oxides in nonpolar media is particularly significant since previous reports on the preparation of mesoporous oxide materials describe synthetic protocols that employ polar (usually aqueous) solvents.[2−6] Presumably, this is due to the fact that these procedures usually entail the hydrolysis of metal alkoxides and utilize the solvent mediated self-assembly of amphiphilic templates, in conjunction with electrostatic and hydrogen-bonding forces. The synthesis of mixed-element oxides in nonpolar solvents allows for use of the thermolytic molecular precursor method, which can give homogeneous mixed-element oxides. The surprising formation of mesoporous oxides from hydrophobic precursors in hydrophobic solvents therefore provides general access to such materials possessing a homogeneous dispersion of more than one element in the framework walls. This work has been previously communicated.[16j]

Results and Discussion

UCB1-ZrSi. A well-studied example of the transformation of a molecular precursor to a mixed-element oxide is the conversion of $Zr[OSi(O^tBu)_3]_4$ (**1**) to $ZrO_2{\cdot}4SiO_2$.[16h] We have been motivated to study zirconia-containing materials due to their refractory properties[19] and their potential use as catalyst supports.[20] Previous experiments have shown that the thermolytic conversion of $Zr[OSi(O^tBu)_3]_4$ results in the production of H_2O and isobutylene as volatile decomposition products. Thus, the thermolysis of **1** may be described by the stoichiometry of eq 1.[16h]

$$Zr[OSi(O^tBu)_3]_4 \xrightarrow{\Delta} ZrO_2{\cdot}4SiO_2 + 12CH_2{=}CMe_2 + 6H_2O \quad (1)$$

When this conversion is carried out in toluene at 135 °C, a monolithic gel is obtained. Air drying of the monolith yields a xerogel, which following calcination at 500 °C for 3 h under O_2 has a surface area of ca. 550 m^2/g. Moreover, the N_2 adsorption−desorption isotherm reveals a high degree of textural mesoporosity, as evidenced by the stark hysteresis loop in the P/P_0 region from 0.6 to 1.0 (Figure 1a).[21] Presumably, this textural mesoporosity arises from the intraaggregate voids defined by the packing of different-sized particles. Moreover, the corresponding pore size distribution is extremely broad, with pore radii ranging from 10 to 500 Å (Figure 1a). As shown in Figure 2a, TEM micrographs of this material reveal the random packing of aggregated particles.

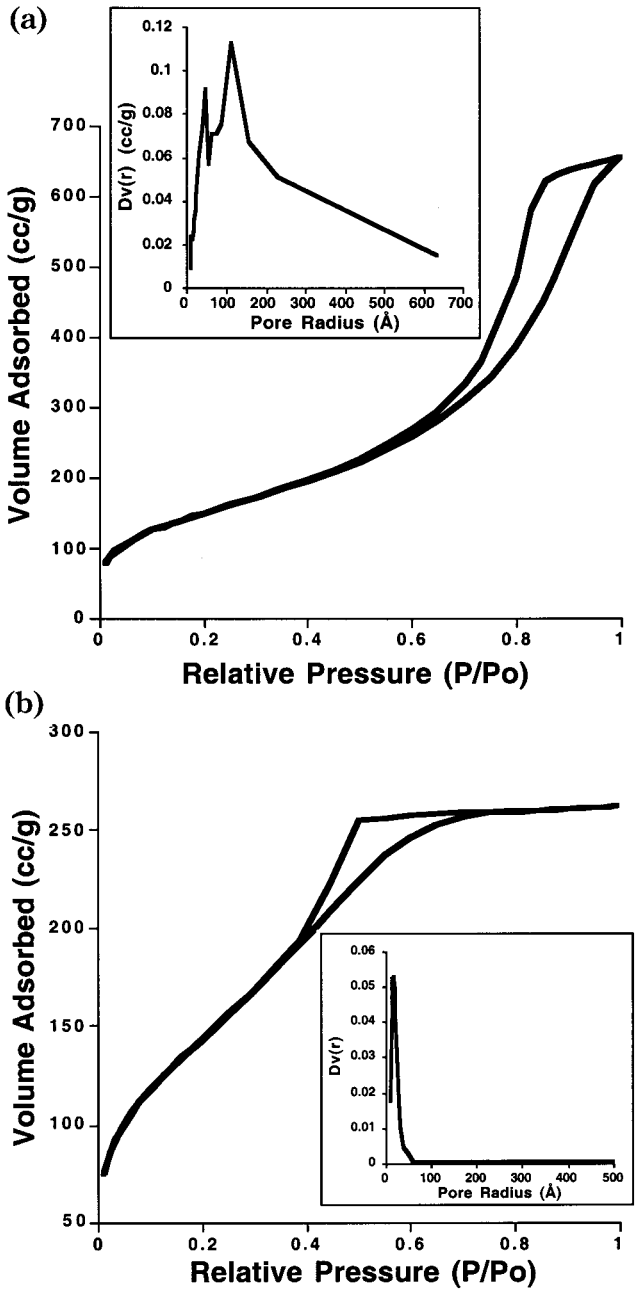

Figure 1. N_2 isotherms for (a) $ZrO_2{\cdot}4SiO_2$ prepared without the addition of a polymeric structure-directing agent and (b) **UCB1-ZrSi** material prepared using the $(H_{33}C_{16})_{10}(OCH_2CH_2)_{10}OH$ diblock copolymer template. The corresponding BJH pore size distributions, shown in the insets, were calculated from the adsorption branches of the isotherms.

Mesostructured $ZrO_2{\cdot}4SiO_2$ was obtained by adding a toluene solution of a poly(ethylene oxide) block copolymer (3−8 wt % relative to toluene) to $Zr[OSi(O^tBu)_3]_4$ (**1**). Several different block copolymers were employed in this study (see Table 1). Thermolysis of this mixture at 135 °C yielded a transparent monolithic gel after several hours. Following air-drying (3−5 d), thermogravimetric analysis (TGA) of the $ZrO_2{\cdot}4SiO_2$/poly-

(19) (a) Simhan, R. G. *J. Non-Cryst. Solids* **1983**, *54*, 335. (b) Yoldas, B. E. *J. Non-Cryst. Solids* **1980**, *38−39*, 81. (c) Paul, A. *J. Mater. Sci.* **1977**, *12*, 2246.

(20) (a) Soled, S.; McVicker, G. B. *Catal. Today* **1992**, *14*, 189. (b) Niwa, M.; Katada, N.; Murakami, Y. *J. Catal.* **1992**, *134*, 340. (c) Bosman, H. J. M.; Kruissink, E. C.; van der Spoel, J.; van den Brink, F. *J. Catal.* **1994**, *148*, 660. (d) Sohn, J. R.; Jang, H. J. *J. Mol. Catal.* **1991**, *64*, 349. (e) Miller, J. B.; Rankin, S. E.; Ko, E. I. *J. Catal.* **1994**, *148*, 673. (f) Miller, J. B.; Ko, E. I. *J. Catal.* **1996**, *159*, 58.

(21) (a) Gregg, S. J.; Sing, K. S. W. *Adsorption, Surface Area and Porosity*, 2nd ed.; Academic Press Inc.: London, 1982. (b) Sing, K. S. W.; Everett, D. H.; Haul, R. A. W.; Moscou, L.; Pierotti, R. A.; Rouqerol, J.; Siemieniewska, T. *Pure Appl. Chem.* **1985**, *57*, 603.

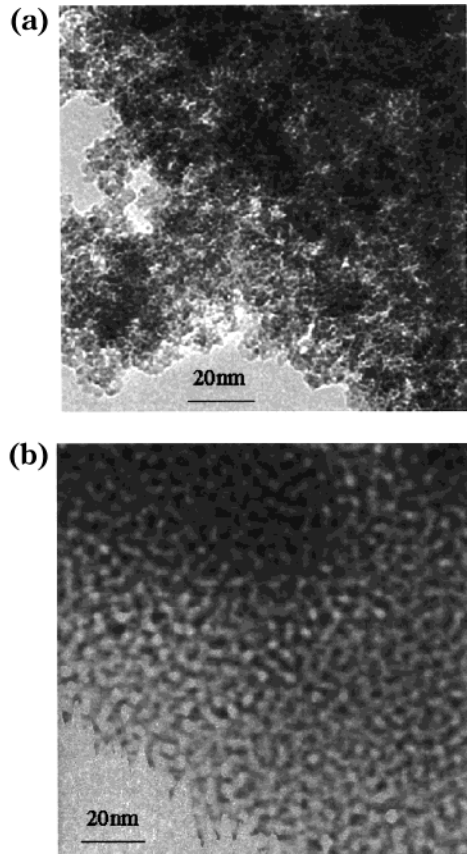

Figure 2. TEM images of (a) ZrO_2·$4SiO_2$ prepared without the addition of a polymeric structure-directing agent and (b) **UCB1-ZrSi** prepared using $(H_{33}C_{16})_{10}(OCH_2CH_2)_{10}OH$ block copolymer. Both samples had been previously calcined to 500 °C under O_2.

mer gel revealed a precipitous weight loss of ca. 50% with an onset temperature of ca. 250 °C. This weight loss corresponds to desorption and decomposition of the block copolymer[22] and suggests that, as expected, the polymer to ZrO_2·$4SiO_2$ ratio is ca. 1:1 (by weight; see Experimental Section).

Calcination of the as-isolated ZrO_2·$4SiO_2$/polymer gel under O_2 for 3 h (500 °C) led to a polymer-free material, **UCB1-ZrSi**. Elemental analysis of **UCB1-ZrSi** revealed that there is no detectable amount of carbon in these materials (i.e. <0.2%). Low-angle powder X-ray diffraction (XRD) patterns for the calcined materials contain a single broad diffraction peak with maxima typically centered at *d* spacings of 105−115 Å. A representative XRD pattern for **UCB1-ZrSi** is shown in Figure 3. These types of broad diffraction peaks usually indicate a lack of long-range crystallographic order and have previously been observed for disordered silicas displaying wormhole type pore channels.[5b,23] Additionally, the diffraction intensity of the **UCB1-ZrSi** materials typically increases slightly after calcination (i.e. removal of the polymeric structure-directing agent). This type of behavior has been previously observed in mesoporous oxide materials and is attributed to an increase in the Bragg-scattering cross section and additional cross-linking of the template-free material.[5b]

The N_2 isotherms for the calcined **UCB1-ZrSi** materials reveal steep adsorptions to a relative pressure (P/P_0) of ca. 0.6 (Figure 1b), after which point there is little additional adsorption. Thus, unlike the untemplated ZrO_2·$4SiO_2$ material, the **UCB1-ZrSi** materials do not contain significant textural mesoporosity. Indeed, the N_2 isotherms for all the **UCB1-ZrSi** materials are indicative of "framework-confined" mesoporosity, in which the pores arise from templated framework channels.[24] However, it should be noted that the desorption hysteresis suggests some necking of the pore channels.[14] The BJH pore size distributions for the mesoporous materials are very narrow relative to the untemplated materials (compare Figure 1a,b). As shown in Table 1, the pore radii for the **UCB1-ZrSi** materials, which were determined from the maximum in the adsorption pore size distribution, appear to increase slightly with increasing polymer molecular weight. Pore volumes and surface areas of these materials typically range from 0.35 to 0.45 cm^3/g and 450−550 m^2/g, respectively, depending on the polymeric structure-directing agent employed (Table 1).

High-resolution TEM experiments on the **UCB1-ZrSi** materials reveal "wormholelike" motifs in which there is no apparent long-range pore order (Figure 2b). Apparently, pores in these materials originate from the space previously occupied by polymer assemblies. However, despite the apparent lack of long-range order, these materials appear to possess relatively uniform channel spacings. Therefore, an estimate of the oxide wall thickness can be made by assuming that the *d* spacing (obtained from low-angle XRD) reflects the channel to channel distance.[25] Thus, using the XRD and pore size data, the wall thickness of the **UCB1-ZrSi** materials was estimated to range from 60 to 85 Å. Indeed the ZrO_2·$4SiO_2$ walls of **UCB1-ZrSi** are considerably thicker (see Table 1) than the silica walls of MCM-41 (10−15 Å)[2a] or those of the mesoporous mixed-element oxides reported by Stucky (35-50 Å).[6a]

Since a primary objective of this work is to synthesize *homogeneous* mesostructured mixed-element oxides, a key issue in the **UCB1-ZrSi** materials is the dispersion of the two inorganic components of the system. Energy-dispersive X-ray spectroscopy (EDX) was used to assess the stoichiometry of the various **UCB1-ZrSi** samples. EDX profiles taken from large (ca. 100 nm) areas confirmed the expected Zr:Si ratio of 1:4 in all the **UCB1-ZrSi** materials. Additionally, local EDX spectroscopy at high spatial resolution was used to probe the distribution of elements in the inorganic framework on a 1 nm scale. For example, the EDX profile of **UCB1-ZrSi** (Figure 4) indicates the relative amount of Zr and Si at 1 nm resolution along a 350 nm piece of the sample (ca. 3.5 nm acquisition intervals). The intensities of the points for both Zr and Si increase over the sampling length due to a steady increase in the thickness of the material. As shown in the inset of Figure 4, the EDX profile confirms the expected Si/Zr ratio (over the entire sample region) in this ZrO_2.$4SiO_2$ material and, there-

(22) (a) Huo, Q.; Margolese, D. I.; Ciesla, U.; Demuth, D. G.; Feng, P.; Gier, T. E.; Sieger, P.; Firouzi, A.; Chmelka, B. F.; Schüth, F.; Stucky, G. D. *Chem. Mater.* **1994**, *6*, 1176. (b) Chen, C.; Li, H.; Davis, M. E. *Microporous Mater.* **1993**, *2*, 17.

(23) Pauly, T. R.; Liu, Y.; Pinnavaia, T. J.; Billinge, S. J. L.; Rieker, T. P. *J. Am. Chem. Soc.* **1999**, *121*, 8835.

(24) Tanev, P. T.; Pinnavaia, T. J. *Chem. Mater.* **1996**, *8*, 2068.

(25) Prouzet, E.; Pinnavaia, T. J. *Angew. Chem., Int. Ed. Engl.* **1997**, *36*, 516.

Table 1. N_2 Porosimetry and XRD Data for UCB1 Materials[a]

oxide	precursor	template	mesoporous mater	surf area (m^2/g)	pore rad. (Å)	d_{100} (Å)	wall thick. (Å)	pore vol (cm/g)
ZrO_2·$4SiO_2$	$Zr[OSi(O^tBu)_3]_4$	none		555	112			1.00
ZrO_2·$4SiO_2$	$Zr[OSi(O^tBu)_3]_4$	$EO_{106}PO_{70}EO_{106}$	**UCB1-ZrSi**	540	22	110	66	0.42
ZrO_2·$4SiO_2$	$Zr[OSi(O^tBu)_3]_4$	$EO_{20}PO_{70}EO_{20}$	**UCB1-ZrSi**	545	20	111	71	0.45
ZrO_2·$4SiO_2$	$Zr[OSi(O^tBu)_3]_4$	$EO_{20}PO_{30}EO_{20}$	**UCB1-ZrSi**	490	13	110	84	0.35
ZrO_2·$4SiO_2$	$Zr[OSi(O^tBu)_3]_4$	$EO_{13}PO_{30}EO_{13}$	**UCB1-ZrSi**	560	13	100	74	0.43
ZrO_2·$4SiO_2$	$Zr[OSi(O^tBu)_3]_4$	$H_{33}C_{16}(OCH_2CH_2)_{10}OH$	**UCB1-ZrSi**	530	16	113	81	0.41
Ta_2O_5·$6SiO_2$	$(EtO)_2Ta[OSi(O^tBu)_3]_3$	none		415	34			0.71
Ta_2O_5·$6SiO_2$	$(EtO)_2Ta[OSi(O^tBu)_3]_3$	$EO_{106}PO_{70}EO_{106}$	**UCB1-TaSi**	400	19	106	68	0.41
Ta_2O_5·$6SiO_2$	$(EtO)_2Ta[OSi(O^tBu)_3]_3$	$EO_{20}PO_{70}EO_{20}$	**UCB1-TaSi**	440	19	110	72	0.44
$AlPO_4$	$(Pr^iO)_2AlO_2P(O^tBu)_2$	none		360	61			1.10
$AlPO_4$	$(Pr^iO)_2AlO_2P(O^tBu)_2$	$EO_{106}PO_{70}EO_{106}$	**UCB1-AlP**	670	39	111	33	1.13
$AlPO_4$	$(Pr^iO)_2AlO_2P(O^tBu)_2$	$EO_{20}PO_{70}EO_{20}$	**UCB1-AlP**	750	33	113	47	1.11
Fe_2O_3·$6SiO_2$	$Fe[OSi(O^tBu)_3]_3$·THF	none		520	25			0.69
Fe_2O_3·$6SiO_2$	$Fe[OSi(O^tBu)_3]_3$·THF	$EO_{106}PO_{70}EO_{106}$	**UCB1-FeSi**	400	12	102	80	0.34
Fe_2O_3·$6SiO_2$	$Fe[OSi(O^tBu)_3]_3$·THF	$EO_{20}PO_{70}EO_{20}$	**UCB1-FeSi**	355	17	105	71	0.34

[a] The corresponding untemplated materials are shown for comparison.

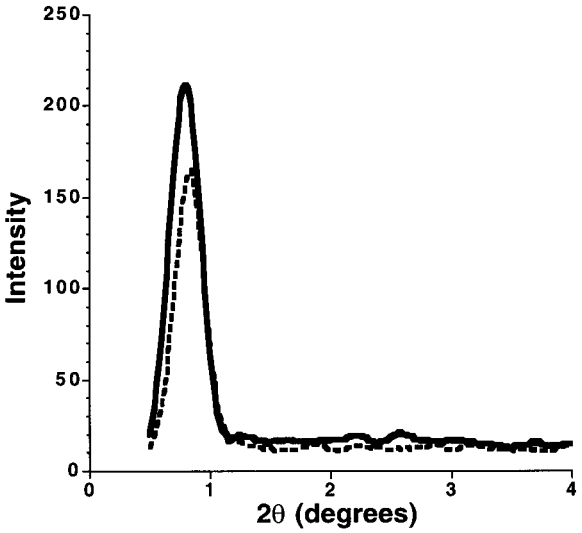

Figure 3. Representative low-angle XRD pattern for **UCB1-ZrSi** prepared using the $EO_{106}PO_{70}EO_{106}$ triblock copolymer structure-directing agent showing uncalcined mesostructured ZrO_2·$4SiO_2$ (dotted line) and calcined ZrO_2·$4SiO_2$ (**UCB1-ZrSi**) (solid line).

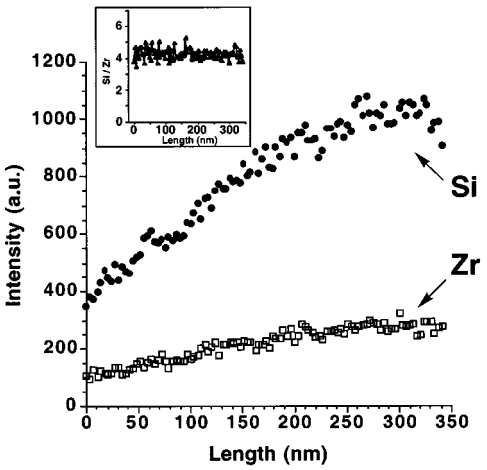

Figure 4. EDX profile of **UCB1-ZrSi** performed using a 10 Å probe at 35 Å intervals (8 s/pt). Points shown as filled circles and open boxes correspond to Si and Zr, respectively. The inset shows the ratio of Si/Zr at each point along the profile for this ZrO_2·$4SiO_2$ material.

fore, provides evidence for a uniform dispersion of elements in the inorganic framework.

To further assess homogeneity in the **UCB1-ZrSi** materials, their crystallization behavior was studied. In ZrO_2·$4SiO_2$ systems there is a correlation between sample homogeneity and the temperature-induced crystallization of zirconia.[26] That is, a well-mixed, amorphous ZrO_2·$4SiO_2$ material will require high-temperature annealing and, hence, substantial diffusion and grain growth for the phase separation of ZrO_2 crystallites. The **UCB1-ZrSi** materials are amorphous until 1100 °C (2 h, under O_2), when nanosized tetragonal zirconia (t-ZrO_2) crystallites are first observed (by XRD). Other amorphous $n$$ZrO_2$·$m$$SiO_2$ systems, made using cohydrolysis of Zr and Si precursors, typically exhibit t-ZrO_2 crystallization between 800 and 1000 °C.[26c,27] These observations therefore indicate that **UCB1-ZrSi** is very homogeneous relative to analogous systems.

Additional characterization of the **UCB1-ZrSi** materials was conducted using solid-state ^{29}Si NMR spectroscopy. These studies provide further evidence that these zirconia-silica materials are well-mixed and contain a significant amount of Zr−O−Si linkages. In an earlier report on untemplated ZrO_2·$4SiO_2$, we characterized peaks observed at lower fields (−90 to −105 ppm) as arising from $Si(OSi)_{4-n}(OZr)_n$ centers (n = 1 or 2; designated as Q^2 and Q^3 sites, respectively).[16h] Solid-state ^{29}Si NMR spectra of **UCB1-ZrSi** contain predominantly Q^2 and Q^3 centers, reflecting a highly homogeneous situation. Interestingly, this spectrum is essentially identical to that observed for untemplated ZrO_2·$4SiO_2$.

The hydrothermal stability of the **UCB1-ZrSi** materials was studied by heating them in refluxing water for 48 h. After isolating the resulting material by filtration, we found that there was no change in the value of the d spacing for the d_{100} peak and only a small loss in surface area (32%). However, the loss in surface area after testing for hydrothermal stability was nearly

(26) Osendi, M. I.; Moya, J. S.; Serna, C. J.; Soria, J. *J. Am. Ceram. Soc.* **1985**, *68*, 135. (b) Garvie, R. C. *J. Phys. Chem.* **1965**, *69*, 1238. (c) Garvie, R. C. *J. Phys. Chem.* **1978**, *82*, 218. (d) Nagarajan, V. S.; Rao, K. J. *J. Mater. Sci.* **1989**, *24*, 2140. (e) Lange, F. F. *J. Mater. Sci.* **1982**, *17*, 235. (f) Heuer, A. H.; Claussen, N.; Kriven, W. M.; Rühle, M. *J. Am. Ceram. Soc.* **1982**, *65*, 642. (g) Skandan, G.; Hahn, H.; Roddy, M.; Cannon, W. R. *J. Am. Ceram. Soc.* **1994**, *77*, 1706.

(27) (a) Jansen, M.; Guenther, E. *Chem. Mater.* **1995**, *7*, 2110. (b) Andrianainarivelo, M.; Corriu, R.; Leclerq, D.; Mutin, P. H.; Vioux, A. *J. Mater. Chem.* **1996**, *6*, 1665. (c) Li, X.; Johnson, P. F. In *Better Ceramics Through Chemistry*; Zelinski, B. J. J., Brinker, C. J., Clark, D. E., Ulrich, D. R., Eds.; Mater. Res. Soc. Symp. Proc. Vol. 180; Materials Research Society: Pittsburgh, PA, 1990; p 355.

identical to that observed for untemplated $ZrO_2 \cdot 4SiO_2$. Additionally, the thermal stability of **UCB1-ZrSi** was studied by heating to 800 °C for 2 h under O_2. After this thermal treatment the **UCB1-ZrSi** materials maintained their mesoporosity (as determined by XRD and N_2 porosimetry) and lost a moderate amount of surface area (ca. 20%). Thus, the molecular precursor route described here allows for the synthesis of highly homogeneous $ZrO_2 \cdot 4SiO_2$ materials that are structurally robust and possess a narrow pore size distribution and thick framework walls.

UCB1-TaSi. Ta_2O_5-containing materials are of interest due to their potential application as solid acid catalysts. When these materials are partially hydrated, they exhibit particularly high acid strengths, thereby making them useful in catalytic reactions that involve water as a byproduct or reagent (e.g. esterifications, condensations, or hydration reactions).[28] Significant effort has been devoted to improving the catalytic properties of Ta_2O_5 by dispersing it on silica supports in order to prevent crystallization of the metal oxide.[29] Thus, we were motivated to synthesize $Ta_2O_5-SiO_2$ materials via a single-source precursor route. In particular, we have prepared $Ta_2O_5 \cdot 6SiO_2$ by thermal decomposition of $(EtO)_2Ta[OSi(O^tBu)_3]_3$ (**2**).[18]

Precursor **2** can be converted in toluene at 140 °C to a monolithic gel. Calcination of this gel (500 °C, 3 h, O_2) leads to a material with a high degree of textural mesoporosity, as evidenced by the large adsorbed volume at high relative pressure in the type IV N_2 isotherm. The corresponding pore size distribution of this material is quite broad with pore radii ranging from 10 to 300 Å.

Addition of a PEO block copolymer (see Table 1) to a toluene solution of $(EtO)_2Ta[OSi(O^tBu)_3]_3$, followed by heating at 145 °C in a sealed ampule, leads to a monolithic gel. Air-drying and calcination of this material yielded a white powder, **UCB1-TaSi**. This material does not contain residual carbon, as determined by elemental analysis. The Ta-containing materials exhibit a single diffraction peak in the low-angle powder XRD pattern (Figure 5) which increases in intensity and becomes sharper after calcination. The single XRD peak indicates that there is a lack of long-range order in these materials. Nitrogen porosimetry data for **UCB1-TaSi** revealed a type IV isotherm and, due to the absence of adsorption at high relative pressures, a lack of textural porosity. Additionally, the pore size distribution for these materials is very narrow, as compared to the untemplated $Ta_2O_5 \cdot 6SiO_2$.

The framework walls of both mesostructured **UCB1-TaSi** materials reported in Table 1 are also very thick (ca. 70 Å) compared to the wall thickness of mesostructured Ta_2O_5 observed by Stucky[6] and Ying[5p] (40 and 14 Å, respectively). TEM images of the **UCB1-TaSi** materials reveal wormhole type pores, which is consistent with the single low-angle diffraction peak in the respective XRD spectra.

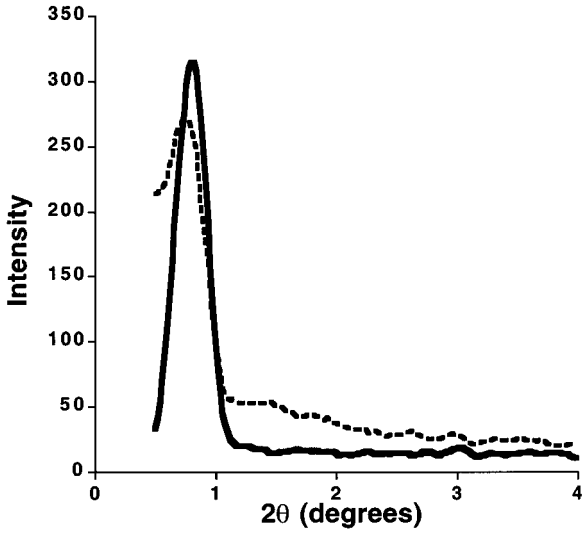

Figure 5. Powder XRD patterns of uncalcined **UCB1-TaSi** (dotted line) and calcined **UCB1-TaSi** (continuous line), prepared using $EO_{106}PO_{70}EO_{106}$ block copolymer.

$Ta_2O_5-SiO_2$ materials typically demonstrate a delayed crystallization of the Ta_2O_5 phase, which indicates an atomically well-mixed multicomponent oxide.[29b] Bulk Ta_2O_5 does not crystallize into its low-temperature phase (L) until 700 °C.[29b] However, crystallization of L-Ta_2O_5 from the amorphous **UCB1-TaSi** did not occur until after this material had been heated to 1100 °C. This delayed crystallization suggests that **UCB1-TaSi** has a relatively uniform distribution of Ta_2O_5 in SiO_2.[29b] Additional support for atomically well-mixed elements in this material was provided by EDX spectroscopy, which confirms the expected Si:Ta ratio of 3:1 with 1000 Å resolution. Local EDX spectroscopy, using a 1 nm probe, provided further support for a homogeneous dispersion of elements. In particular, the elemental composition of a **UCB1-TaSi** sample > 400 nm in length was probed at 10 nm intervals. At each point in this EDX profile, the Ta:Si ratio is approximately 1:3. The **UCB1-TaSi** materials are very thermally stable, maintaining their mesoporosity (by XRD and N_2 porosimetry) and losing 26% of their surface area after treatment at 800 °C for 2 h under O_2.

UCB1-FeSi. Interest in $Fe_2O_3-SiO_2$ materials stems from their use as catalysts in (for example) the Fischer–Tropsch process[30] and their use in recording and memory devices.[31] Thus, we targeted the mixed-element oxide precursor $Fe[OSi(O^tBu)_3]_3 \cdot THF$[32] (**3**) as a single-source precursor for $Fe_2O_3-SiO_2$ materials. Thermolysis of **3** in toluene solution led to a brown monolithic gel, which after air-drying afforded the untemplated xerogel. The xerogel obtained from **3** possesses a broad pore size distribution (ca. pore radii 10–300 Å) and significant textural mesoporosity as determined from analysis of the nitrogen isotherm and TEM micrographs.

Mesostructured $Fe_2O_3-SiO_2$ was obtained by addition of a triblock copolymer (see Table 1) to a toluene solution

(28) Tanabe, K. J.; Misono, M.; Ono, Y.; Hattori, H. In *New Solid Acids and Bases: Their Catalytic Properties*; Studies in Surface Science and Catalysis Vol. 51; Delmon, B., Yates, J. T., Eds.; Elsevier: New York, 1989.

(29) (a) Yoshida, H.; Tanaka, T.; Funabiki, T.; Yoshida, S. *Catal. Today* **1996**, *28*, 79. (b) Guiu, G.; Grange, P. *Bull. Chem. Soc. Jpn.* **1994**, *67*, 2716.

(30) Pommier, B.; Reymond, J. P.; Teichner, S. J. *J. Phys. Chem.* **1985**, *89*, 203.

(31) (a) Chaneac, C.; Tronc, E.; Jolivet, J. P. *J. Mater. Chem.* **1996**, *6*, 1905. (b) Ennas, G.; Musinu, A.; Piccaluga, G.; Zedda, D.; Gatteschi, D.; Sangregorio, C.; Stanger, J. L.; Concas, G.; Spano, G. *Chem. Mater.* **1998**, *10*, 495.

(32) The precursor $Fe[OSi(O^tBu)_3]_3$ crystallizes with one molecule of THF, as described in ref 18.

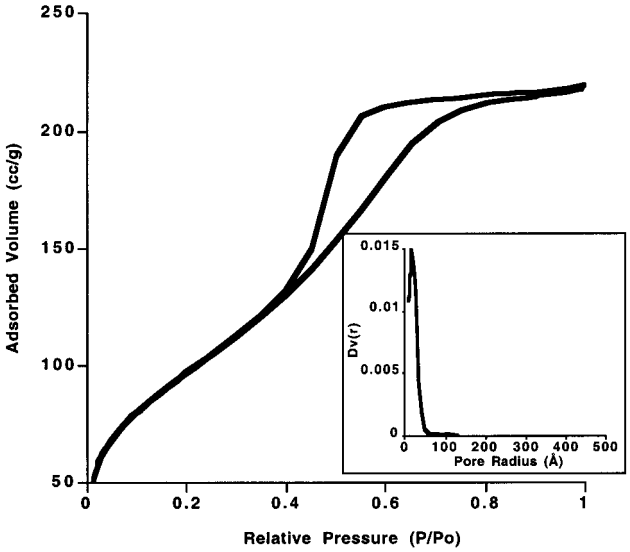

Figure 6. N_2 isotherm for a **UCB1-FeSi** material prepared using the $EO_{20}PO_{70}EO_{20}$ triblock copolymer structure-directing agent. The corresponding BJH pore size distribution, shown in the inset, was calculated from the adsorption branch of the isotherm.

of **3**. After thermolysis of this solution at 135 °C, a monolithic gel was formed. Following air-drying and calcination of this material, a brown powder (**UCB1-FeSi**) was obtained. Elemental analysis revealed that this material does not contain residual carbon. Nitrogen porosimetry analysis revealed that the pore size distribution of **UCB1-FeSi** is significantly more narrow than that for the corresponding untemplated $Fe_2O_3-SiO_2$ material. The N_2 isotherm and corresponding pore size distribution for a **UCB1-FeSi** material are shown in Figure 6. The surface areas of the mesostructured $Fe_2O_3-SiO_2$ materials (ca. 400 m^2/g) are somewhat lower than those of the untemplated material (520 m^2/g).

Low-angle XRD patterns for the **UCB1-FeSi** materials contain a single broad diffraction peak that is similar in *d* spacing and shape to **UCB1-ZrSi** and **UCB1-TaSi.** TEM micrographs of **UCB1-FeSi** reveal a wormhole type pore structure with framework walls that are very thick (80−85 Å). EDX spectroscopic analysis of the mesostructured $Fe_2O_3{\cdot}6SiO_2$ showed that the Si:Fe ratio is approximately 1:3 (see Experimental Section). The **UCB1-FeSi** materials are amorphous until they are annealed to 1000 °C, at which time α-Fe_2O_3 crystallites are visible by powder XRD. In other $Fe_2O_3-SiO_2$ systems, crystallization of an iron oxide phase is first observed (by XRD) after annealing the material to 700 °C.[31b] Thus, these mesostructured $Fe_2O_3-SiO_2$ materials (**UCB1-FeSi**) appear to contain an atomically well-mixed dispersion of the two oxide phases. Additionally, the mesoporosity in the **UCB1-FeSi** materials is preserved (by XRD and N_2 porosimetry) after calcining at 800 °C for 2 h under O_2, as this thermal treatment results in a moderate loss (31%) in surface area. The **UCB1-FeSi** materials are most likely structurally robust due to their thick framework walls.

UCB1-AlP. Aluminophosphate materials have applications as catalysts, catalyst supports,[33] ion exchangers, and adsorbants.[34] Since there has been widespread use of $AlPO_4$ zeolites in catalysis, it is expected that analogous mesoporous materials will inevitably prove useful.[35] Thus, several research groups have reported the use of supramolecular templates in the synthesis of mesoporous aluminophosphates.[36,37] In particular, charged or neutral alkylamine surfactants have been employed to construct $AlPO_4$ materials with pore radii of 6−20 Å.[36] Additionally, several aluminophosphate/surfactant composites have been reported in which the surfactant could not be successfully removed without collapse of the framework walls.[35,37]

The synthesis and thermolytic transformation of molecular precursors to $AlPO_4$ materials has previously been described.[16i,18] On the basis of that work, xerogels derived from $[Al(O^iPr)_2O_2P(O^tBu)_2]_4$ were obtained by thermolysis (in toluene solution) at 135 °C, which led to a monolithic gel. After air-drying and calcination (500 °C, O_2, 3 h), the $AlPO_4$ xerogel exhibited a type IV N_2 isotherm with a H3 hysteresis (Figure 7a), which is indicative of a tenuous assemblage of particles that define slit-shaped pores.[21] Indeed, TEM studies on these materials corroborate the interpretation of the N_2 porosimetry data. The corresponding pore size distribution is quite broad with pore radii ranging from 10 to 800 Å. Additionally, the surface area of the untemplated $AlPO_4$ xerogel is 360 m^2/g, which is also a fairly typical value for aluminophosphate materials made via sol−gel protocols.[16i]

Mesostructured $AlPO_4$ materials were made by the addition of a toluene solution of a block copolymer ($EO_{106}PO_{70}EO_{106}$ or $EO_{20}PO_{70}EO_{20}$) to $[Al(O^iPr)_2O_2P(O^tBu)_2]_4$. Heating this mixture in a sealed ampule at 135 °C led to a monolithic gel. Calcination (500 °C, O_2, 3 h) yielded **UCB1-AlP** as a white amorphous powder (by powder XRD). The N_2 isotherm for **UCB1-AlP** (Figure 7b) is type IV with a hysteresis loop that is intermediate between H1 and H2. Comparison of the N_2 isotherms of untemplated $AlPO_4$ and **UCB1-AlP** (Figure 7a,b) suggests that the pore structures of these two materials are dramatically different. Indeed the pore sizes of **UCB1-AlP** are quite narrow and show an increase in their maxima with increasing polymer length (see Table 1). Further, the average pore radii for

(33) (a) Mostafa, M. R.; Youssef, A. M. *Mater. Lett.* **1998**, *34*, 405. (b) Parida, K.; Mishra, T. *J. Colloid Interface Sci.* **1996**, *179*, 233. (c) Petrakis, D. E.; Hudson, M. J.; Pomonis, P. J.; Sdoukos, A. T.; Bakas, T. V. *J. Mater. Chem.* **1995**, *5*, 1975. (d) Glemza, R.; Parent, Y. O.; Welsh, W. A. *Catal. Today* **1992**, *14*, 175. (e) Costa, A.; Deya, P. M.; Sinisterra, J. V.; Marinas, J. M. *Can. J. Chem.* **1980**, *58*, 1266. (f) Cheung, T. T. P.; Willcox, K. W.; McDaniel, P. M.; Johnson, M. M. *J. Catal.* **1986**, *102*, 10.

(34) (a) Mishra, T.; Parida, K. M.; Rao, S. B. *Sep. Sci. Technol.* **1998**, *33*, 1057. (b) Kandori, K.; Ikeguchi, N.; Yasukawa, A.; Ishikawa, T. *J. Colloid Interface Sci.* **1998**, *202*, 369. (c) Kandori, K.; Ikeguchi, N.; Yasukawa, A.; Ishikawa, T. *J. Colloid Interface Sci.* **1996**, *182*, 425.

(35) Tiemann, M.; Fröba, M.; Rapp, G.; Funari, S. S. *Chem. Mater.* **2000**, *12*, 1342.

(36) (a) Kimura, T.; Sugahara, Y.; Kuroda, K. *Microporous Mesoporous Mater.* **1998**, *22*, 115. (b) Zhao, D.; Luan, Z.; Kevan, L. *Chem. Commun.* **1997**, 1009. (c) Cabrera, S.; Haskouri, J. E.; Guillem, C.; Beltrán-Porter, A.; Beltrán-Porter, D.; Mendioroz, S.; Marcos, M. D.; Amorós, P. *Chem. Commun.* **1999**, 333. (d) Holland, B. T.; Isbester, P. K.; Blanford, C. F.; Munson E. J.; Stein, A. *J. Am. Chem. Soc.* **1997**, *119*, 6796. (e) Luan, Z.; Zhao, D.; He, H.; Klinowski, J.; Kevan, L. *J. Phys. Chem. B* **1998**, *102*, 1250. (f) Kimura, T.; Sugahara, Y.; Kuroda, K. *Chem. Commun.* **1998**, 559. (g) Kimura, T.; Sugahara, Y.; Kuroda, K. *Chem. Mater.* **1999**, *11*, 508. (f) Eswaramoorthy, M.; Neeraj, S.; Rao, C. N. R. *Microporous Mesoporous Mater.* **1999**, *28*, 205.

(37) (a) Oliver, S.; Kuperman, A.; Coombs, N.; Lough A.; Ozin, G. A. *Nature* **1995**, *378*, 47. (b) Sayari, A.; Karra, V. R.; Reddy, J. S.; Moudrakovski, I. L. *Chem. Commun.* **1996**, 411. (c) Gao, Q.; Chen, J.; Xu, R.; Yue, Y. *Chem. Mater.* **1997**, *9*, 457. (d) Feng, P.; Xia, Y.; Feng, J.; Bu, X.; Stucky, G. D. *Chem. Commun.* **1997**, 949. (e) Fröba, M.; Tiemann, M. *Chem. Mater.* **1998**, *10*, 3475.

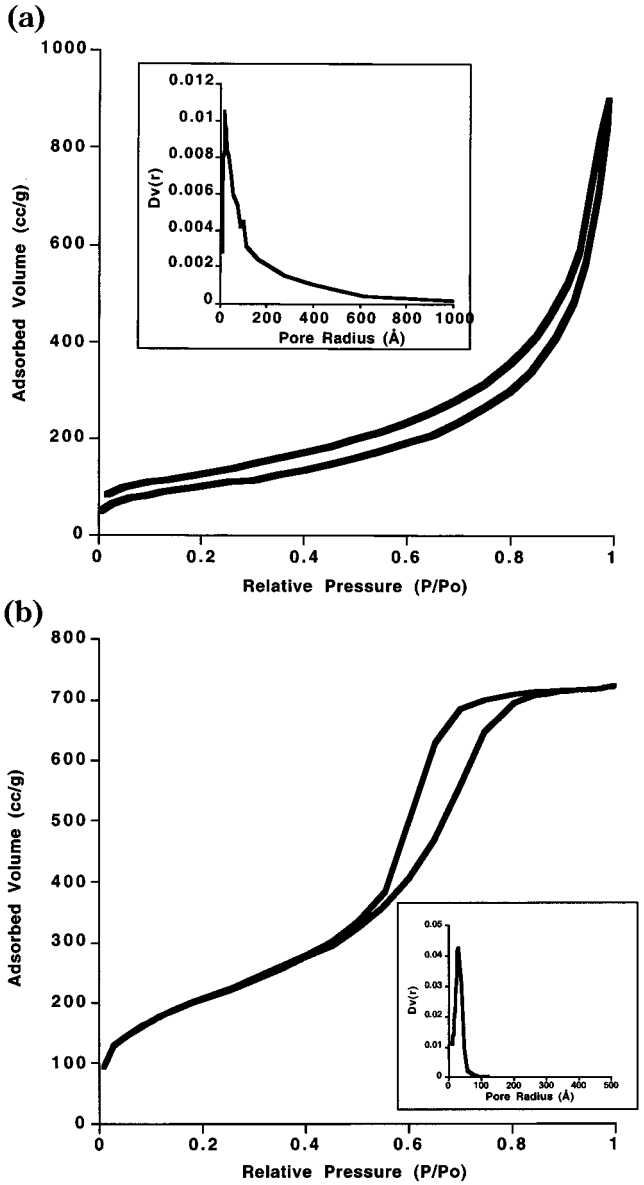

Figure 7. N_2 isotherm for (a) $AlPO_4$ prepared without the addition of a polymeric template and (b) **UCB1-AlP** prepared using the $EO_{20}PO_{70}EO_{20}$ triblock copolymer structure-directing agent. The corresponding BJH pore size distributions, shown in the insets, were calculated from the adsorption branches of the isotherms.

the **UCB1-AlP** materials reported in Table 1 (39 and 33 Å) are significantly larger than those reported for other mesostructured $AlPO_4$ materials (10−18 Å).[36a] The **UCB1-AlP** materials also have a particularly well-defined N_2 isotherm, as is evident by observation of two distinct adsorption processes, (i) monolayer coverage and (ii) capillary condensation ($P/P_0 \approx 0.6$).

Low-angle powder XRD patterns for the **UCB1-AlP** materials contain a single diffraction peak with *d* spacings of 111 and 113 Å, which again indicates the likelihood of disordered wormhole type pores. Indeed, TEM analysis of the mesostructured materials reveal pore structures with wormhole type motifs. Using the XRD data and the pore size maxima from N_2 porosimetry analyses, the walls of the **UCB1-AlP** materials were determined to be relatively thick (33−47 Å). Analogous $AlPO_4$ materials made by different synthetic protocols (i.e. using alkylammonium surfactants) typically have framework walls of 10−20 Å.[36] The **UCB1-AlP** materials have the expected Al:P ratio of 1:1, as determined using EDX spectroscopy. Additionally, these mesoporous materials are extremely stable, remaining amorphous by powder XRD until crystallites of the tridymite form of $AlPO_4$ become apparent after annealing to 1200 °C. Moreover, the mesoporosity in the **UCB1-AlP** materials is preserved even after thermal treatment to 800 °C for 2 h under O_2, as determined by XRD and the shape of the N_2 porosimetry isotherm. This heat treatment resulted in a 52% loss of surface area. The thermal stability of **UCB1-AlP** is particularly notable since many of the $AlPO_4$−surfactant composites reported to date are not thermally stable and incur loss of mesoscopic order under relatively mild conditions.[35]

To further characterize the **UCB1-AlP** materials, ^{27}Al and ^{31}P MAS NMR spectroscopy was performed. The ^{27}Al NMR spectrum reveals an intense peak at 42 ppm and another resonance at −11 ppm. The downfield resonance corresponds to tetrahedrally coordinated Al in an AlO_4 structural unit.[36e,38] Octahedrally coordinated Al, arising from $Al(OP)_4(OH_2)_2$ type structural units, most likely gives rise to the resonance at ca. −11 ppm in the ^{27}Al NMR spectrum.[38] The ^{31}P NMR spectrum displays a single peak at −25 ppm, which can be attributed to $P(OAl)_4$ tetrahedra and is outside the range for P−O−P linkages.[38,39] Thus, the **UCB1-AlP** materials appear to have a highly regular structure involving −Al−O−P− linkages in the framework.

Concluding Remarks

In summary, a general route for synthesizing mesoporous mixed-element oxides using single-source molecular precursors and polymeric structure-directing agents has been described. This synthetic strategy features the opportunity to engineer porous materials with more complex stoichiometries and atomically well-mixed oxide structures, relative to alternative protocols previously employed. As a demonstration of this synthetic approach, the mixed-element oxides $ZrO_2{\cdot}4SiO_2$, $Ta_2O_5{\cdot}6SiO_2$, $Fe_2O_3{\cdot}6SiO_2$, and $AlPO_4$ have been synthesized with pore radii of 10−39 Å, depending on the polymeric structure-directing agent employed. Additionally, these **UCB1** materials have relatively thick framework walls (33−85 Å) compared to MCM-41 silicas (10−15 Å)[2a] and the few mixed-element oxides that have been reported (35-40 Å).[6a]

Previous reports on template-assisted mesoporous metal oxide formation describe synthetic protocols that employ highly polar, usually aqueous, reaction solvents.[6b] Polar solvents are expected to be key components in the formation of mesoporous oxides, because the cooperative assembly of the template and inorganic species is believed to occur via electrostatic and hydrogen-bonding interactions.[6] In addition, polar reaction solvents would seem to favor use of poly(alkylene oxide) block copolymers as templates, since they are known to self-assemble into well-defined mesophases in aqueous media.[40] It is therefore significant that mesostructures develop in a nonpolar environment during formation of

(38) Engelhardt, G. E.; Michel, D. *High-Resolution Solid-State NMR of Silicates and Zeolites*; John Wiley and Sons Ltd.: New York, 1987.
(39) Sayari, A.; Moudrakovski, I.; Reddy, J. S. *Chem. Mater.* **1996**, *8*, 2080.

the **UCB1** materials, especially since little is know about the phase behavior of poly(alkylene oxide) block copolymers in nonaqueous solvents.[40]

The mechanism by which the **UCB1** materials form is not yet known, but presumably mesostructural order results from assembly of the copolymer with the molecular precursor in a nonpolar solvent or from interaction of the copolymer with decomposition products resulting from thermolysis of the precursor. Potentially relevant considerations have been reported recently by Soler-Illia and Sanchez,[41] who have observed that hydrolyses of transition metal alkoxides in the presence of poly(ethylene oxide)-based surfactants produce monoliths or xerogels displaying wormholelike mesophases at low water concentrations. The authors postulated that, under these conditions, the ether moieties in the polymer chains coordinate to the transition metal species, and these interactions promote polymer unfolding. Furthermore, it was suggested that the ether groups serve as nucleation sites for the growing inorganic phase. Additional condensation of inorganic species around the alkylene oxide scaffold then lead to gels with a vermicular pore structure. Finally, the Sanchez study revealed that there is no significant change in the wormholelike mesostructure of the metal oxides when the size of the polymeric structure-directing agent is dramatically changed (as determined by TEM and XRD).

Interactions between the poly(ether) structure-directing agents and the molecular precursors employed in the current study are quite reasonable, since the coordination of ethers (e.g., THF) to metal−$OSi(O^tBu)_3$ complexes is often observed.[16h,18] Thus, addition of the precursor to a copolymer template probably results in some interaction, and subsequent thermolytic decomposition of the metal complexes yields reactive nucleation sites which may adhere even more strongly to the polymer. Condensation of the polymerizing inorganic species then leads to a gel in which the inorganic framework is templated by the copolymer surfactant. This templating may result from preferential condensation of the precursor within certain blocks of the copolymer (e.g., in the more hydrophobic, disordered, and less dense PO segments of the EO−PO−EO copolymers in which the EO blocks are expected to be more condensed). The vermicular structure would then result from thermolytic transformation of the precursor, combined with calcination to remove the template. However, at this time we cannot rule out an anisotropic space-filling mechanism in which the polymers indiscriminately fill the voids between condensing inorganic species. In this scenario, the polymers would simply prevent colloidal inorganic particles (emanating from thermolytically decomposed molecular precursors) from growing randomly and, subsequently, yielding a material with a broad pore size distribution. Given that our molecular precursors are expected to interact with ether functionalities quite strongly, it seems unlikely that the polyalkene oxide structure-directing agents play such a benign role in the synthesis of the **UCB1** materials.

Future studies using molecular precursors and polymeric structure-directing agents should focus on the use of molecular precursors (or combinations thereof) that yield mesoporous materials with complex elemental compositions and useful catalytic properties. The preparation and use of block copolymer structure-directing agents with blocks that differ substantially in hydrophobicity should be applied to the synthesis of new generations of **UCB1** materials. In addition, the mechanistic proposal made herein will be investigated using various spectroscopic techniques and a variety of molecular precursors, block copolymers, and solvents.

Experimental Section

General Methods. All reactions were performed under an inert dinitrogen atmosphere using standard Schlenk techniques. Toluene was distilled from potassium. Elemental analyses were performed by Mikroanalytisches Labor Pascher or the College of Chemistry Microanalytical Facility. TEM micrographs were taken on a JEOL CM-200 at 200 KV by depositing the finely ground gel on a lacey "type A" carbon-coated Cu grid obtained from Ted Pella Inc. Energy-dispersive X-ray (EDX) spectra were taken on a Gatan detector connected to the electron microscope (electron beam size 100−1000 Å). The N_2 porosimetry data were collected on a Micromeritics ASAP 2010 or a Quantachrome Autosorb-1 instrument using either a 60 point or 80 point analysis, after degassing for a least 24 h at 120 °C. The pore size distributions were calculated using the Barrett−Joyner−Halenda (BJH) method and the adsorption branch of the isotherm.[21] The average pore radius (Table 1) was determined from the global maximum in the BJH pore size distribution. The pore volume was taken at $P/P_0 = 0.974$. Thermolyses were performed using a Lindberg 1700 °C or a Lindberg 1200 °C three-zone tube furnace. Heat treatments were carried out with flowing (100 cm^3 min^{-1}) oxygen (99.6%). The heating rate was 10 °C min^{-1} to the specified temperature, which was typically maintained for 2 h. The samples were then cooled at a rate of 10 °C min^{-1}. Thermal analyses were performed on a TA Instruments SDT 2960 Simultaneous DTA-TGA. Powder X-ray diffraction was performed on a Siemens D5000 diffractometer. Elemental analyses were performed at the College of Chemistry Microanalytical Facility. The solid-state NMR spectra were aquired by Drs. Kevin Ott and Andrea Laboriau at the Los Alamos National Laboratory. The Pluronic block copolymers F127 ($EO_{106}PO_{70}EO_{106}$, $M_{av} = 12600$), P123 ($EO_{20}PO_{70}EO_{20}$, $M_{av} = 5800$), P65 ($EO_{20}PO_{30}EO_{20}$, $M_{av} = 3400$), and L64 ($EO_{13}PO_{30}EO_{13}$, $M_{av} = 2900$) were generous gifts from BASF (Mt. Olive, NJ). The block copolymer $H_{33}C_{16}(OCH_2CH_2)_{10}OH$ (Brij 56) was obtained from Aldrich. The preparations of $Zr[OSi(O^tBu)_3]_4$,[16h] $[Al(O^iPr)_2O_2P(O^tBu)_2]_4$,[16i] $(EtO)_2Ta[OSi(O^tBu)_3]_3$ (**2**),[18] and $Fe[OSi(O^tBu)_3]_3{\cdot}THF$[18] are described elsewhere.

UCB1-ZrSi. In a typical preparation, 0.20 g of the block copolymer was dissolved in 6.0 mL of dry toluene. After the polymer fully dissolved, the solution was transferred to a glass tube that was interfaced through a Cajon adapter to a glass fitting with an N_2 inlet and septum, containing 0.60 g of $Zr[OSi(O^tBu)_3]_4$. This mixture was freeze−pump−thawed at least 4 times and then sealed with a torch under vacuum. The glass ampule was then placed in an oven that was preheated to 135 °C and heated overnight. Typical gel times were 3−24 h. Adding a catalytic amount of $AlCl_3$ (ca. 0.5 mg) significantly reduced gel times but seemed to have no effect on the properties of the **UCB1-ZrSi** material. The monolith was isolated by opening the ampule and allowing the gel to air-dry in a Petri dish for 3−5 d at room temperature, after which time the gel had shrunk by ca. 70% and cracked into several pieces. The gel was then powdered and calcined at 500 °C under O_2 in a tube furnace for 3 h. Anal. by EDX Si/Zr. Found for $ZrO_2{\cdot}4SiO_2$: Si, 81; Zr, 19. Anal. Found for C and H: C, <0.2; H, 1.66.

UCB1-TaSi. A synthetic protocol similar to that used for **UCB1-ZrSi** was employed. However, in a typical preparation,

(40) Chu, B.; Zhou, Z. In *Nonionic surfactants: polyalkylene block copolymers*; Nace, V. M., Ed.; Surface Science Series Vol. 60; Marcel Dekker: New York, 1996.

(41) Soler-Illia, G. J. de A. A.; Sanchez, C. *New J. Chem.* **2000**, *24*, 493.

0.15 g of block copolymer, 0.46 g of $(EtO)_2Ta[OSi(O^tBu)_3]_3$, and 6.0 mL of toluene were used. A monolith normally formed within 3 h, but the gel was heated overnight (135 °C). Anal. by EDX Si/Ta. Found for $Ta_2O_5{\cdot}6SiO_2$: Si, 75; Ta, 25. Anal. Found for C and H: C, <0.2; H, 2.37.

UCB1-FeSi. A synthetic protocol similar to that used for **UCB1-ZrSi** was employed. However, in a typical preparation, 0.28 g of block copolymer, 0.40 g of $Fe[OSi(O^tBu)_3]_3{\cdot}THF$, and 5.4 mL of toluene were used. A monolith normally formed within 2 h, but the gel was heated overnight (135 °C). Anal. by EDX Si/Fe. Found for $1/2Fe_2O_3{\cdot}3SiO_2$: Si, 75; Fe, 25. Anal. Found for C and H: C, <0.2; H, 1.43.

UCB1-AlP. A synthetic protocol similar to that used for **UCB1-ZrSi** was employed. However, in a typical preparation, 0.50 g of block copolymer, 0.60 g of $[Al(O^iPr)_2O_2P(O^tBu)_2]_4$, and 7.0 mL of toluene were used. A monolith normally formed within 2 h, but the gel was heated overnight (135 °C). Anal. by EDX Al/P. Found for $AlPO_4$: Al, 51; P, 49. ^{27}Al CP MAS NMR: δ 42.2 (AlO_4), −11.5 ($Al(OP)_4(OH_2)_2$). ^{31}P CP MAS NMR: δ ∠25 ($P(OAl)_4$). Anal. Found for C and H: C, 0.2; H, 3.11.

Acknowledgment. This work was supported by the Director, Office of Basic Energy Sciences, Chemical Sciences Division, of the U.S. Department of Energy under Contract No. DE-AC03-76SF00098. We thank Drs. Kevin Ott and Andrea Laboriau for the acquisition of solid-state NMR spectra and are grateful to Chris Nelson at the National Center for Electron Microscopy for technical assistance.

CM010068T